NANO FEATURES CONSTRUCTION ON PDMS MICROFLUIDIC DEVICES:

Towards a micro-Fuel Cell

Abstract

This project explores the construction of a Hydrogen Peroxide Single Compartment Microfluidic Fuel Cell. A detailed process flow is presented highlighting the cell construction via two-photon lithography and electrodeposition. Cathode and anode sit close to each other with layered and porous structure to reduce energy lost. The electrode pattern is written by Nanoscribe that precisely control the shape and size with negative photoresist and can be further removed by plasma treatment. Anode is made of nickle through electrical deposition while cathode is thin tungsten trioxide layer covering outside Ni with strong adhesion. The final micro-device achieves power densities of 27.6 mW/cm^2 and 3.6 W/cm^3.

Christian Barresi, Yuzhe Li

E241

1 Table of Contents

1 Introduction 1

1.1 Motivation 1

1.2 Benefits to the SNF Community 1

2 Process Flow 3

3 Fabrication and Experimental Results 4

3.1 SiO_2 Growth 4

3.2 Photolithography 4

3.3 Metal Evaporation and Liftoff 5

3.4 Two-Photon lithography 5

3.4.1 Nanoscribe 6

3.4.2 Development and Plasma Treatment 8

3.5 Support Structure Electrodeposition 8

3.6 Template Removal 9

3.7 Cathode Electrodeposition 9

3.8 PDMS Channel Construction 10

4 Results and Discussion 10

4.1 Support Structure 10

4.2 Cathode 11

4.3 Fuel Cell Performance 13

5 Conclusion 14

6 Future Work 15

7 Acknowledgement 15

8 Budget 15

9 References 16

Figure 1: (a) H2O2 Microfluidic SCFC (b) Electrodes Intended Porous Structure 1
Figure 2: Process Flow Overview. Generation of a Single compartment fuel cell using two-photon lithography and electrodeposition 3
Figure 3: KLayout design. (a) Array structure design for exposing 4 structures per wafer. (b) Individual structure design, with contact pads for the cathode and anode. (c) Cathode and anode base pattern—structure measures 290 µm x 600 µm. 4
Figure 4: Wafer after lift-off and metallization 5
Figure 5: Two Photon Photolithography Diagram[4] 5
Figure 6: (a) Neural Network Architecture (b) Regression Space 7
Figure 7: SolidWorks STL files. (a) 5 µm pore radius (b) 20 µm pore radius 8
Figure 8: Regression Curve for estimating Ni growth Thickness based on number of Cycles. 1 Hz frequency, 50% Duty Cycle 9
Figure 9: (a) Microchannel mold (b) PDMS with embedded microchannel structure (c) Microchannel Structure inside PDMS 10
Figure 10: SEM Images of 5 µm porous Ni Structure. (a) Ni overflow structure (b) SEM depth imaging showing the 3D structure (c) Hydrogen Pitting on Nickel Structure 11
Figure 11: (a) Optical Image of 20 µm porous Ni Structure with WO_3 cathode. Cathode and anode can be visually determined by darker contrast of WO_3 with respect to Ni. (b) Cathode XPS: high current deposition. (c) Cathode XPS: low current deposition 12
Figure 12: (a) Cathode XPS Surface survey (b) Cathode XPS 100 nm depth Survey (c) Cathode XPS 100 nm depth Tungsten Profile. As expected, due to the argon sputtering, more metallic tungsten appears. (d) Cathode XPS 100 nm depth Nickel Profile. 13
Figure 13: (a) Polarization Curve (b) Power Density Curve 14

Table 1: Nanoscribe DOE 6

1 Introduction

1.1 Motivation

Fuel cells are an alternative renewable energy source that can fill different niches. One such niche is microelectronics, where a simple single compartment fuel cell could be built to satisfy the energy needs in laptop, biosensor and so on. In this work, we are exploring the Hydrogen Peroxide (H_2O_2) Single Compartment Microfluidic Fuel Cell (SCFC)—using Tungsten Trioxide (WO_3) as cathode and Nickel (Ni) as anode materials—due to peroxide's capacity to acts as both, fuel and oxidizer.

By creating a microfluidic cell (**Figure 1** (a)) with embedded nano/micro-features—a method that influences electrolyte flow—we intend on maximizing the electrolyte surface coverage, reactant replenishment, and product removal. By affecting the diffusion of reactants, products, and ions, the microfluidic cell will have positive changes in the electrodes double layer. In addition, by affecting these parameters and working in the nano/micro-scale, we expect to develop high volumetric power densities. Finally, to simplify construction of the device, this work will explore having the electrodes as the embedded nano/micro-features (**Figure 1** (b)) that will influence the electrolyte flow through the microfluidic cell.

H_2O_2 unique property to serve as an oxidizer and fuel creates a "mixed potential" at the fuel cell's cathode—simultaneous competing H_2O_2 reduction reaction (HPRR), H_2O_2 oxidation reaction (HPOR), and oxygen reduction reaction (ORR)—inhibiting the fuel cell's maximum power output[1,2]. By controlling the flow rate and gap size between the layers under PDMS, reactor can reduce O_2 generation.

$$\text{HPRR: } H_2O_2 + 2H^+ + 2e^- \rightarrow 2H_2O,\ E° = 1.77\ \text{V vs SHE}$$

$$\text{HPOR: } H_2O_2 \rightarrow 2H^+ + 2e^- + O_2,\ E° = 0.695\ \text{V vs SHE}$$

$$\underline{\text{Cell Reaction: } 2H_2O_2 \rightarrow 2H_2O + O_2,\ \Delta E° = 1.08\ \text{V}}$$

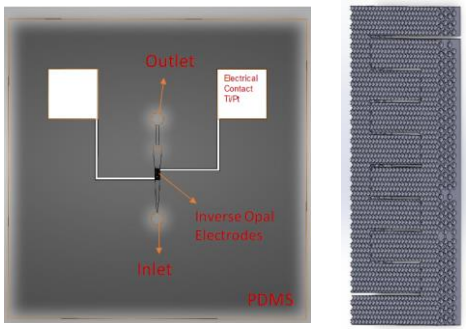

Figure 1: *(a) H_2O_2 Microfluidic SCFC (b) Electrodes Intended Porous Structure*

1.2 Benefits to the SNF Community

This work benefits SNF in two aspects. First, our work with the Nanoscribe will offer an understanding on how to print 3D structures on patterned metallic substrates. A standard operating procedure (SOP) will be developed to characterize the following:

1. Two-photon polymerization writing parameters using Design of Experiments to functionalize the laser power and speed for different metal substrates.
2. Nanoscribe positioning and alignment for writing in patterned structures
3. SU-8 negative template resist removal compatible with microfluidic devices

Second, our work will offer a pathway—by means of an SOP contained in this work—for developing microfluidic fuel cells, including electrodeposition parameters and removal of sacrificial templates.

2 Process Flow

This project explores the generation of a microfluidic single compartment fuel cell via photolithography, Dip in Laser two-photon lithography, and electrodeposition. The overview of the process flow is described below and shown on **Figure 2**.

1. Deposit Resist
2. Expose and develop substrate pattern
3. Deposit metal contact and perform lift-off
4. Deposit IP-S negative photoresist
5. Expose negative sacrificial template and develop
6. Plasma treatment for increasing SU-8 hydrophilicity
7. Deposit metal in sacrificial template interstices by electrodeposition
8. Remove sacrificial template via plasma cleaning
9. Deposit cathode catalyst via electrodeposition
10. Create microchannel using PDMS

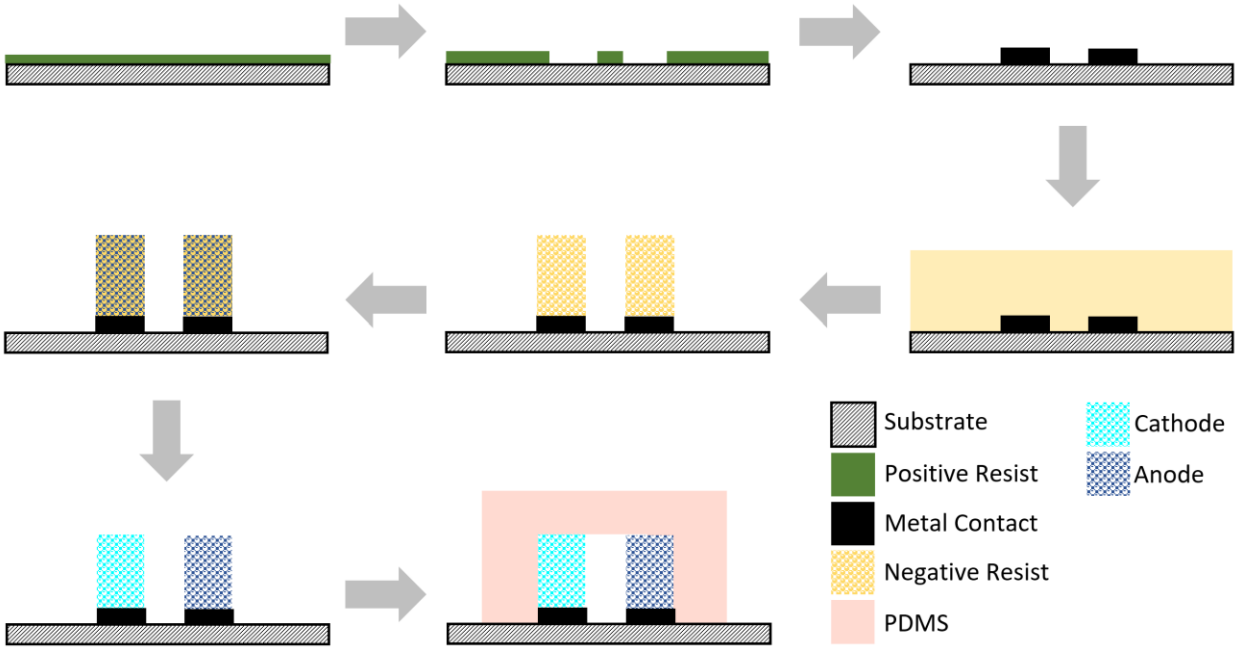

Figure 2: *Process Flow Overview. Generation of a Single compartment fuel cell using two-photon lithography and electrodeposition*

3 Fabrication and Experimental Results

3.1 SiO_2 Growth

Silicon dioxide growth was performed on the 4 inch <100> silicon wafer to establish an electrical insulating barrier to prevent electrical connection between the cathode and the anode. Calculations for the growth were performed using the Massoud Model and solving the differential equation in Matlab. A total thickness of 300 nm of oxide was grown under wet atmosphere at 1000°C using the Tylan9 furnace.

a. $Massoud\ Model$: $\frac{dx}{dt} = \frac{B}{2x+A} + Ce^{-E/kT}e^{-x/L}$ (1)

i. x = Oxide Thickness
ii. C = 6.5 u µm /min
iii. E = 2.37 eV
iv. L = 7nm
v. B, A: Deal Grove Model Constants[3]

3.2 Photolithography

Wafers were primed with HMDS (Hexamethyldisilazane) prior to coating with resist to enhance the bond between the wafer surface and the photoresist. An automatic track system was used to dispense and cure an even coating of positive photoresist. For this process, 1.6 µm of Shipley 3612 photoresist was deposited onto the substrate. Photoresist exposure was achieved using Heidelberg MLA 150-2 direct write photolithography with default write parameters. This tool has a minimum resolution of 0.60 µm, therefore the minimum feature sizes of our structure were kept above 1 µm. The mask was designed using KLayout.

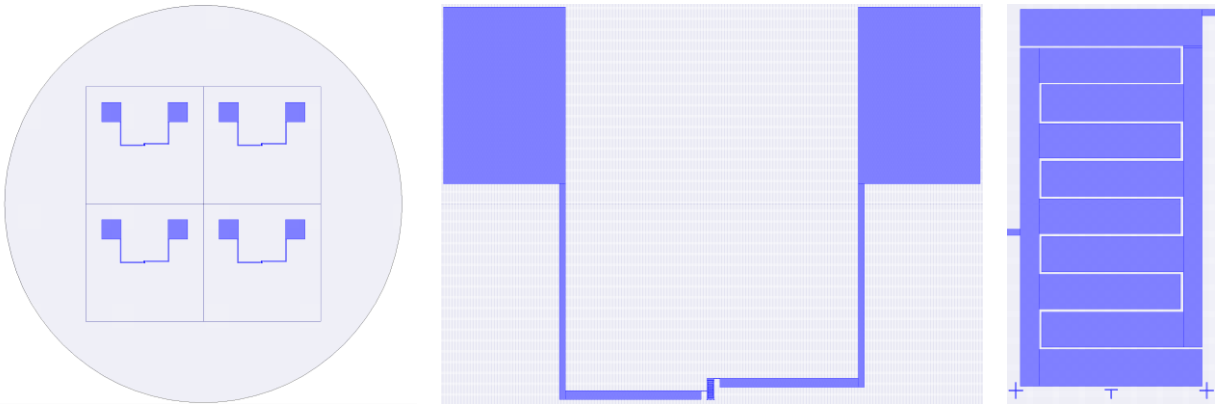

Figure 3: *KLayout design. (a) Array structure design for exposing 4 structures per wafer. (b) Individual structure design, with contact pads for the cathode and anode. (c) Cathode and anode base pattern—structure measures 290 µm x 600 µm.*

After exposure, the resist was baked and developed using an automatic track system.

3.3 Metal Evaporation and Liftoff

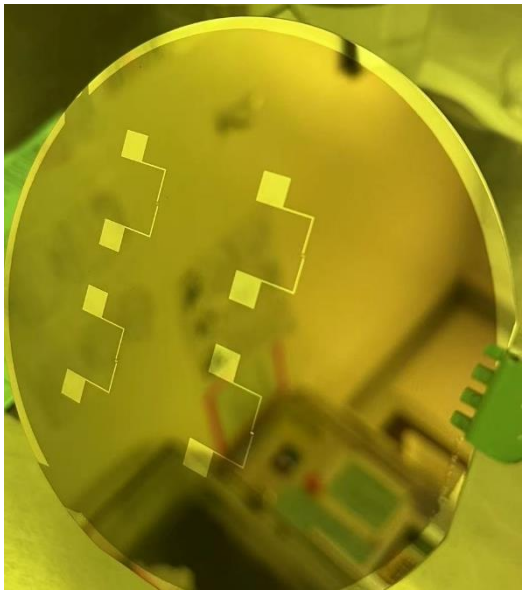

To achieve successful lift-off on our inverse pattern with sacrificial photoresist, Electron Beam Evaporation—a directional process with minimal sidewall buildup—was selected using the Lesker E-Beam Evaporator. Two layers of metals were selected for this process to create the anode and cathode electrical system. First 180 nm of Titanium were deposited to act as adhesion promoter and current collector. The second layer consisted of 10 nm of Palladium or Platinum to prevent surface corrosion and act as the base for the subsequent electrodeposition process.

The sacrificial photoresist was removed under sonication with acetone, followed by cleaning with methanol and isopropanol.

Figure 4: *Wafer after metal deposition on mask and lift-off*

3.4 Two-Photon lithography

The two-photon photopolymerization technique is versatile and applicable for fabrication in the nanoscale regime[4]. Resins are polymerized by absorbing two photons at a longer wavelength, usually in the near-infrared (NIR) spectral region. Most of the commercially available polymers have negligible linear absorption in the near-infrared (NIR) region, and therefore the laser beam penetrates deeply into materials and directly induces polymerization from inside without initiating any photochemical process outside of the focal volume enabling high 3D spatial resolution[4].

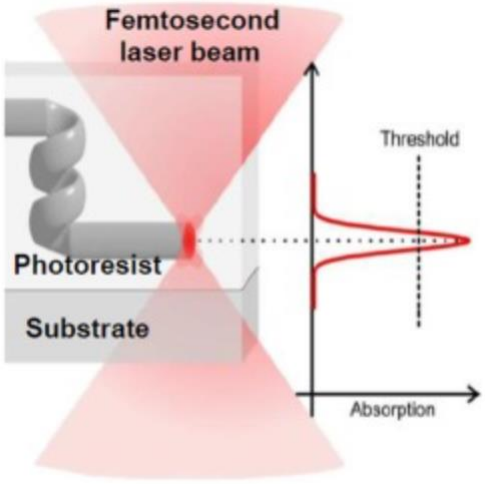

Figure 5: *Two Photon Photolithography Diagram[4]*

The controlled laser beam is tightly focused onto a photocurable resin through a high numerical aperture (NA) objective lens, which consequently creates photo density profiles with an equal number of photons at all cross sections on the focused spot. The resin is exposed only within the focal volume of the beam generally known as voxel[4]. The process of two-photon polymerization (TPP) is restricted only to this volume giving rise to a 3D resolution[4].

3.4.1 Nanoscribe

The Nanoscribe is a TPP tool used to create the negative templates for our cathode and anode. TPP is a non- linear optical process that can absorb two photons at the same time by acting photo-initiator on the resist and polymerized the resist locally. It can be used to create complex 3D structure with feature size down to 100 nm. For this project IP-S negative photoresist was selected alongside the Nanoscribe's 25x NA 1.4 objective in Dip in Laser Lithography (DiLL) configuration. This setup boasts a resolution of 1 µm and lateral size writing distribution of 400 µm in the XY plane and 150 µm in the XZ/YZ plane[5].

Nanoscribe has a plethora of writing parameters, but the principal parameters dictating the quality of the structure are laser power and laser writing speed. For the project, design of experiment (DOE) was implemented to study the effect of four different parameters—laser contour power, laser contour speed, laser solid/scaffolding power, and laser solid/scaffolding speed.

Pattern	Contour Speed	Contour Power	Solid Spped	Solid Power	Structure Quality	Write Time
000A	55000	55	55000	100	0	2.05
000a	55000	55	55000	40	0	2.05
+−+−	100000	30	100000	40	1	2.25
−+−+	10000	80	10000	100	-1	3.07
0A00	55000	80	55000	70	1	2.05
A000	100000	55	55000	70	0	2.04
00A0	55000	55	100000	70	0	2.25
+−++	100000	30	100000	100	-1	2.25
++++	100000	80	100000	100	-1	2.25
+++−	100000	80	100000	40	0	2.25
−+−−	10000	80	10000	40	1	3.07
−−−−	10000	30	10000	40	1	3.07
−−−+	10000	30	10000	100	-1	3.07
0	55000	55	55000	70	0	2.05
++−−	100000	80	10000	40	-1	3.04
+−−−	100000	30	10000	40	1	3.04
−−++	10000	30	100000	100	0	2.28
a000	10000	55	55000	70	1	2.08
0a00	55000	30	55000	70	0	2.05
−++−	10000	80	100000	40	0	2.28
−+++	10000	80	100000	100	0	2.28
+−−+	100000	30	10000	100	-1	3.07
−−+−	10000	30	100000	40	0	2.28
00a0	55000	55	10000	70	-1	3.04
0	55000	55	55000	70	1	2.05
++−+	100000	80	10000	100	-1	3.04

Table 1: *Nanoscribe DOE*

From these experiments performed on a Titanium substrate, a regression response surface was obtained that correlates the effects of the four writing parameters with structure quality—(-1) for unacceptable, (0) for acceptable, and (1) for Best Quality. This regression response surface was obtained using a 2-layer

neural network—designed in JMP—with the architecture shown on Figure 6. Results from the regression boasted R-squared values greater than 90%.

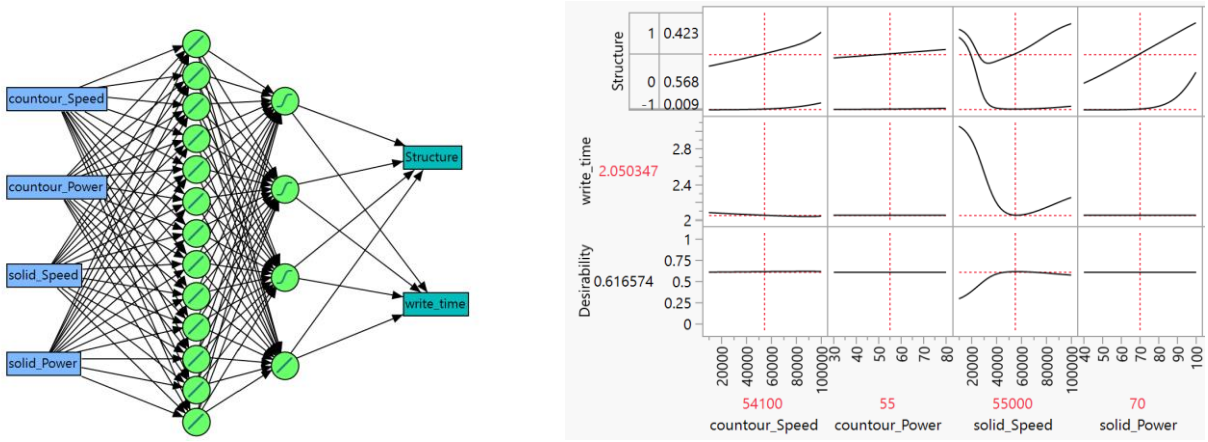

Figure 6: *(a) Neural Network Architecture (b) Regression Space*

Further experimentation found a correlation between our response surface results and the ratio between the extinction coefficients of Ti: Pt and Pd—where laser power was proportional to this ratio and laser speed is inversely proportional to the ratio.

All Nanoscribe negative template structures were design in Solidworks and processed for 3D printing using DeScribe software. These templates were constructed such that they were able to achieve the following goals:

a. High porosity structure
b. Maximize surface area
c. Minimize structure volume
d. Cover metal connections position not intended for electrodeposition process
e. Ensure electrical isolation between the cathode and anode structures
f. Provide structural support and ease of removal
    a. This goal was studied by performing the 3D prints as solid structures and scaffolding structures. The Solid structure provides more structural stability, but it is harder to remove. The scaffolding structure is easier to remove but provides less structural support.

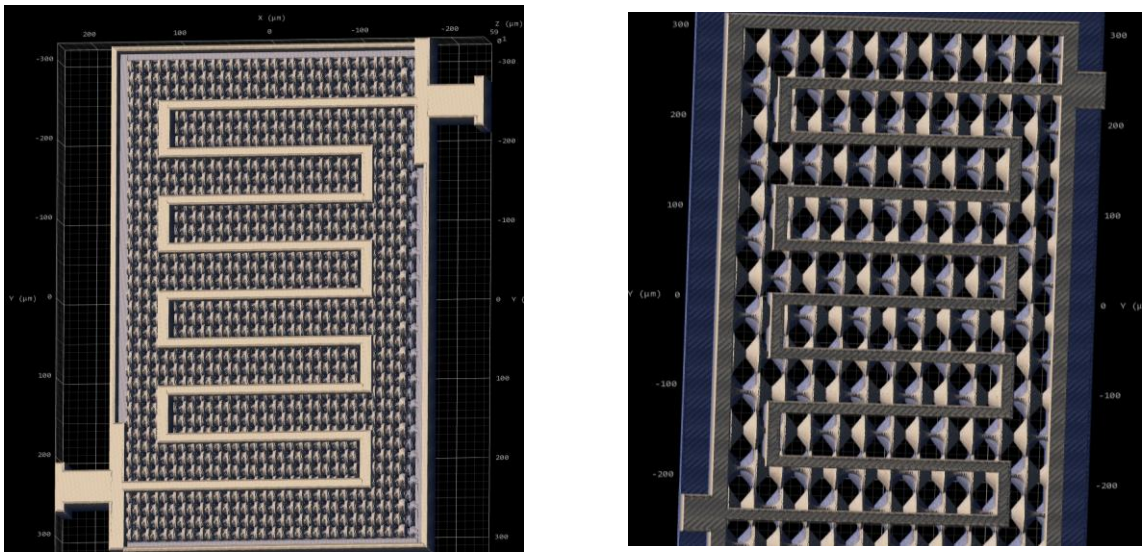

Figure 7: *SolidWorks STL files. (a) 5 µm pore radius (b) 20 µm pore radius*

3.4.2 Development and Plasma Treatment

The 3D printed structures in IP-S photoresist were developed by immersing the print in SU-8 developer for 20 minutes followed by two consecutive 5 minutes isopropanol immersions and subsequent air drying. Once the isopropanol had finished evaporating, the cross-linked SU-8 3D structures were subjected to plasma treatment to increase their hydrophilicity. The plasma treatment was performed using Samco P300 with the following parameters: 250 W, 50 SCCM O_2, and 30 Pa, for a total of 5 minutes. Both the solid and scaffolding structures maintained their structural integrity after the plasma treatment.

3.5 Support Structure Electrodeposition

The positive 3D structure in the template interstices was formed by electrodeposition. For this process, Nickel electrodeposition was selected due to being a good support metal, availability of chemical recipes, growth rate, deposition quality, and good catalytic affinity for our anodic reaction. An all-Nickel Sulfate solution—in accordance with reference [6]—was selected, consisting of 300 g/L Nickel Sulphate, 40 g/L Boric Acid, and 2 mg/L Sodium Dodecyl Sulphate (SDS).

To maximize the electrolyte penetration in the 3D template and improve the quality of the resulting structure, several steps were taken:

a. The electrodeposition process occurred under a vacuum. Potential was applied after no bubbles were observed, minimizing the amount of gases in the solution.
b. The solution was maintained at 60 C to improve the deposition rate and lower the required current.
c. The deposition was controlled via pulsed potentiometry—using a Gamry 1010B Potentiostat—with a frequency of 5 Hz and 50% duty cycle. Current was limited to 28 mA-cm^{-2}. This allowed for electrolyte replenishment across the double layer and prevented hydrogen gas from coming out of solution. This electrodeposition process is done in Mechanical Engineering Research Laboratory (Xiaolin Zheng's lab) within a filter flask.

d. Surfactant (SDS) was added to minimize hydrogen pitting and allow the electrolyte to penetrate all crevices.

e. Electrodeposition time was approximated using DOE and controlling the number of cycles and current density to measure resultant thickness. The testing data points are set by JMP. Different current regions or frequencies were not explored since the relationship between the experiment and alternative experimental conditions are proportional. Gamry Potentiostat is set at 1Hz frequency, 50 V and 50% duty cycle with cycles and current as two variables.

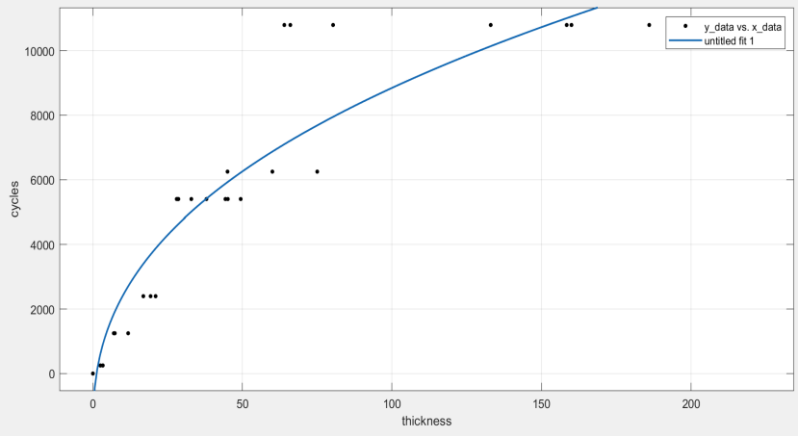

Figure 8: *Regression Curve for estimating Ni growth Thickness based on number of Cycles. 1 Hz frequency, 50% Duty Cycle*

3.6 Template Removal

After performing experiments on SU-8 removal via piranha solution (Water: sulfuric acid: H_2O_2 = 5:1:1), high temperature (500℃) polymer oxidation, and plasma treatment—it was determined that from the three methods, plasma treatment was the least harmful to our structures. Based on a paper investigating the removal of cross-linked SU-8[7], we determined to use a mixture of O_2/SF_6 plasma for the sacrificial negative template removal. For this process we used Samco P300 with the following parameters: 250 W, 50 SCCM O_2, 3 SCCM SF_6, and 30 Pa, for a total of 5 minutes (plasma on time). Due to the lack of cooling in the tool, multiple plasma cycles (plasma on- open chamber to cool down – plasma on) had to be performed to prevent the structure from collapsing due to heating and expansion from the polymer. Normally, most structures would be completely cleaned after 4 cycles. The removal degree was observed through optical microscope. Successfully removing template samples have Ni sitting in the gap position and very little blurry white color resist.

3.7 Cathode Electrodeposition

For catalysis, only the surface interaction between the catalyst and the reactants is of importance. Therefore, just a few nanometers of catalyst deposited onto the nickel support structure on the cathode side, will suffice the catalysis requirements. The catalyst selected for the cathode was tungsten trioxide (WO_3), due to being able to be selectively deposited by electrodeposition and good catalysis properties for the cathodic reaction.

The electrolyte[8], composed of 0.01M Sodium Tungstate, 0.005M Aluminum Chloride Hexahydrate, and 0.05 M Hydrogen Peroxide was sonicated while adding hydrochloric acid until obtaining a clear solution and a pH of ~1.

To maximize the electrolyte penetration in the 3D structure and improve the quality of the resulting catalyst, several steps were taken:

a. The electrodeposition process occurred under a vacuum. Potential was applied after no bubbles were observed, minimizing gas in the solution.
b. The solution was maintained at 40 C to improve the deposition rate.
c. A shock to the system was conducted with pulsed potentiometry for 10 cycles—using a Gamry 1010B Potentiostat—at a frequency of 100 Hz, 10% duty cycle, and 250 mA-cm^{-2}. This deposition was followed by another pulsed potentiometry at a frequency of 5 Hz, 50% duty cycle, and 50 mA-cm^{-2} for a duration of 3 minutes.
    a. This deposition can be visually verified by chromatic change during the active pulses.

3.8 PDMS Channel Construction

The microfluidic channel structure was embedded in PDMS. PDMS mold shape is firstly written by Nanoscribe shown in the first image in Fig.9. The center of the mold is a concave to cover microfluidic channel. PDMS was mixed with a Base: Crosslink ratio of 10:1 in the Thinky Mixer. Then the PDMS solution was poured over a salinized mold containing the microfluidic channel structure and was placed in a vacuum chamber until the PDMS solution was completely degassed. The mold with PDMS was cured at 100 C for 4 hours.

The cured PDMS was removed from the mold and placed in Samco P300—250 W, 50 SCCM O_2, and 30 Pa, for a total of 5 minutes—with the silicon wafer containing the electrodes for O_2 plasma bonding. After the Plasma treatment, the PDMS microchannel was aligned with the electrode's structure and bonded together.

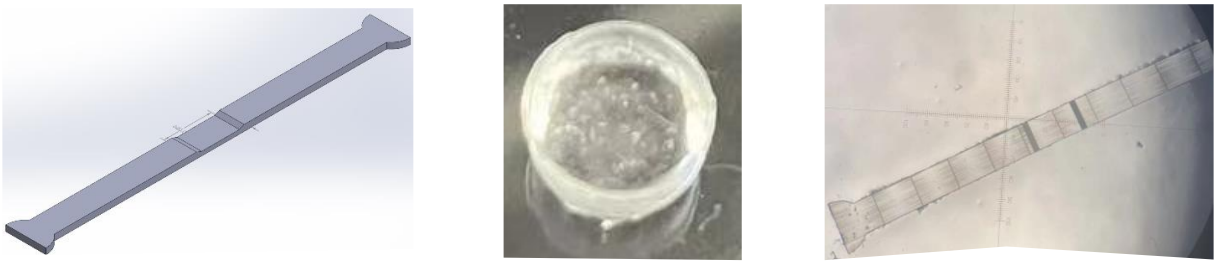

Figure 9: *(a) Microchannel mold (b) PDMS with embedded microchannel structure (c) Microchannel Structure inside PDMS*

4 Results and Discussion

4.1 Support Structure

The electrochemical Nickel deposition parameters were crucial in determining the quality of the resultant structure. With parameters such as current, deposition time, pulse frequency, and recipe having the highest impact on the resulting structure—creating a strong 3D structure as seen on **Figure 10** (b) or a weak structure with vacant sites due to detrimental effects.

1. **High Current:** It was observed that high current densities regardless of the pulse frequency or duty cycle, tended to cause overflow of Nickel and poor penetration of the electrolyte. An adverse effect of overgrowth is the short-circuiting of the anode and cathode as observed in **Figure 10** (a), which renders the fuel cell structure useless.
2. **Low Current:** Low current was essential to prevent hydrogen gas buildup in the cell and thus preventing hydrogen pitting—**Figure 10**(c)—or gas bubbles from blocking the electrolyte from reaching all the crevices in the negative template. An adverse effect of low current is that it increases the deposition time significantly.

3. **Pulse Frequency (50% Duty Cycle):** Very low pulse frequencies (less than 1 Hz) approximate a constant current deposition, which does not allow for electrolyte replenishment at the double layer interface and promotes gas buildup. Two effects that inhibits deposition of the 3D structure. At high pulse frequencies (greater than 100 Hz), the change in deposition speed does not allow for electrolyte replenishment nor gas removal—essentially observing the same impact as constant deposition.
4. **Surfactant addition:** Including the right surfactant, is another factor that increases the wettability of the electrolyte and allows it to penetrate deeper in the 3D structure. A feature that becomes vital as the pore size of the negative template decreases. In addition, it prevents hydrogen pitting and gas buildup by lowering the surface binding energy. The scum layer caused by surfactant can be removed by water.

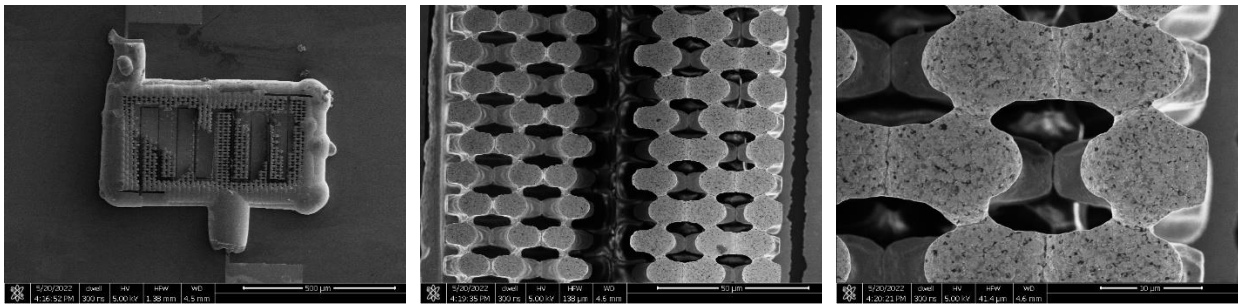

Figure 10: *SEM Images of 5 µm porous Ni Structure. (a) Ni overflow structure (b) SEM depth imaging showing the 3D structure (c) Hydrogen Pitting on Nickel Structure*

4.2 Cathode

The cathode electrodeposition, due to its nature of only being a couple of nanometers thick, did not suffer as sensitive to parameter variation as the support structure electrodeposition. The most crucial element to perform a good deposition for the cathode was to ensure electrolyte penetration and achieve the current that develops no visible Hydrogen gas—therefore allowing the electrolyte to cover the surface of the support structure. The second crucial element was to obtain metallic tungsten in the electrodeposition to increase the conductivity of the catalyst. Figure 11 shows XPS results we done to check the material contents form the WO_3 electrodeposition at both high and low current density. Fig.11 (a) indicates the darker half is WO3 deposited cathode and the lighter part is Ni-only anode. Fig.11 (b) is deposition under high current, the outcome material contains both WO_3 and W metal while Fig.11 (c) in low current density, it only has WO_3. The W metal help improve the conductivity. Thus, increasing conductivity of catalyst can be achieved by doping the solution with aluminum and performing the deposition at relatively high current densities in a short amount of time.

(a) Optical Image

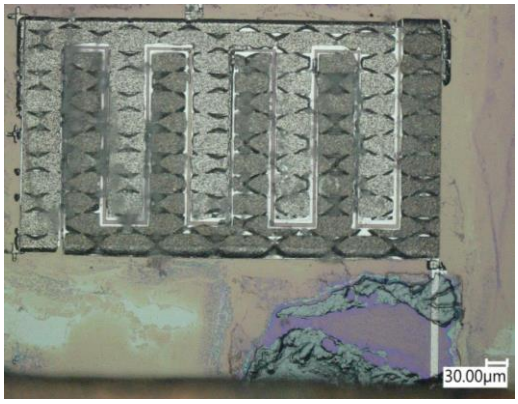

(b) XPS: High Current Density

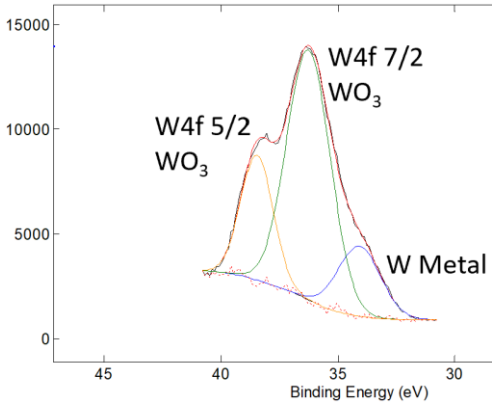

(c) XPS: Low Current Density

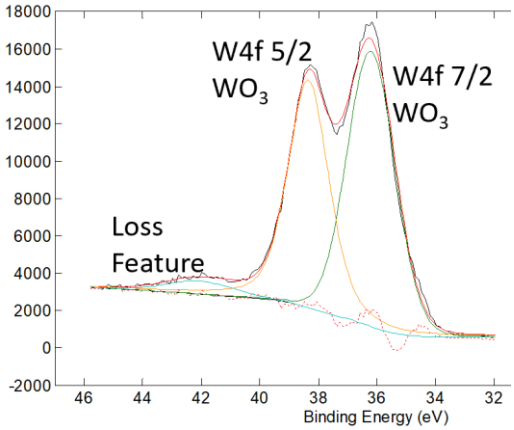

Figure 11: *(a) Optical Image of 20 µm porous Ni Structure with WO_3 cathode. Cathode and anode can be visually determined by darker contrast of WO_3 with respect to Ni. (b) Cathode XPS: high current deposition. (c) Cathode XPS: low current deposition*

Additionally, **Figure 12** shows via a XPS depth profile that tungsten trioxide is deposited on top of the Nickel support structure. Because XPS is a surface sensitive analysis, penetrating between 10~20 nm, the Nickel of the support structure does not appear in the initial survey.

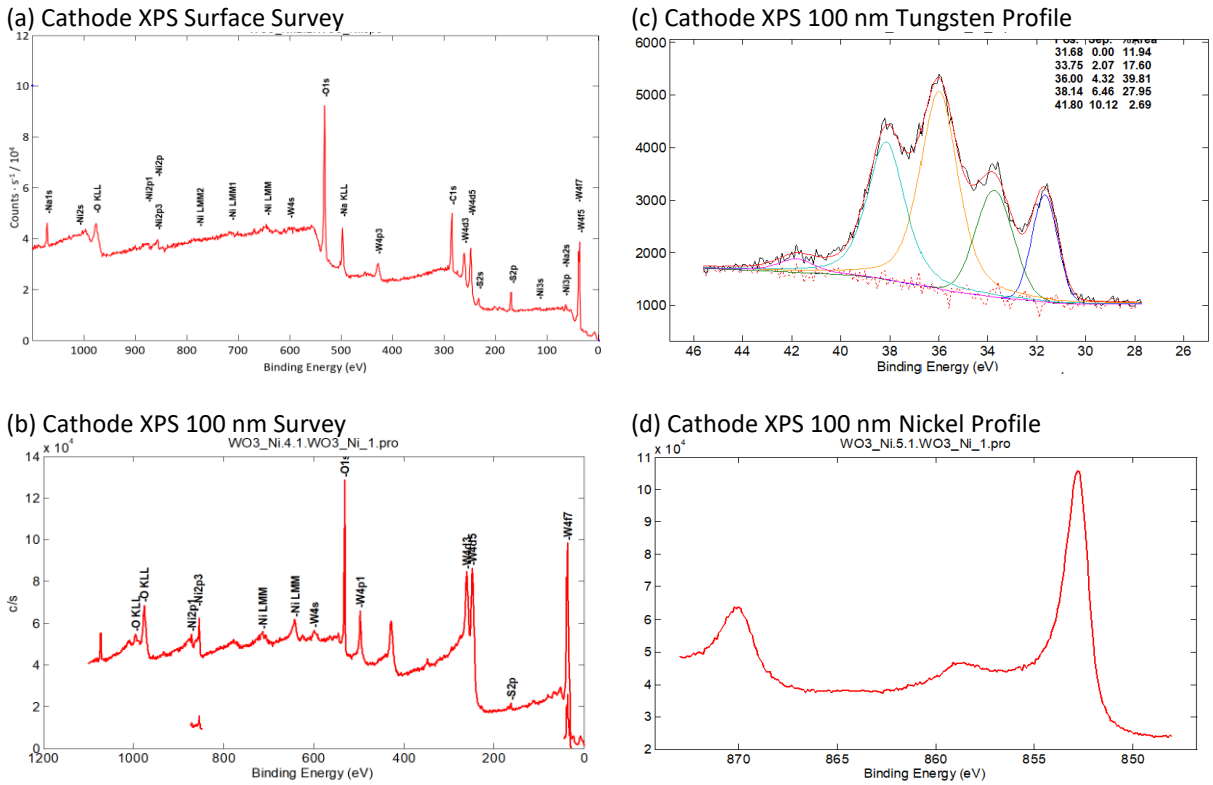

Figure 12: *(a) Cathode XPS Surface survey (b) Cathode XPS 100 nm depth Survey (c) Cathode XPS 100 nm depth Tungsten Profile. As expected, due to the argon sputtering, more metallic tungsten appears. (d) Cathode XPS 100 nm depth Nickel Profile.*

4.3 Fuel Cell Performance

The H_2O_2 single compartment fuel cell performance was evaluated in a two-electrode configuration using a Gamry 1010B Potentiostat. The cell performed under constant flow of electrolyte—consisting of 0.5 M H_2O_2 and 0.1 M HCl—through the microchannel. The performance was measured using the potentiostat automatic polarization curve function and the potentiostat manual linear sweep voltammetry function.

Figure 13 shows the polarization curve and power density curve for the fuel cell. In this figure the open circuit potential of the curve is approximately 400 mV. A deviation from the theoretical value of 1.1 Vis caused by a "mixed potential" suffered by the fuel at the cathode[1,2]. Nonetheless, its maximum power density is approximately 27.6 mW-cm^{-2} and its active volume power density is 3.6 W-cm^{-3}. Values of power density that surpasses by a great margin the current values found in literature[9,10], and volumetric power densities comparable to solid oxide fuel cells. These power density values can be explained due to the high porosity of the 3D structure at the micro-scale—which allows a high surface area under constant replenishment of electrolyte and minimizes the distance the reactants need to travel due to its proximity, thereby allowing high current densities.

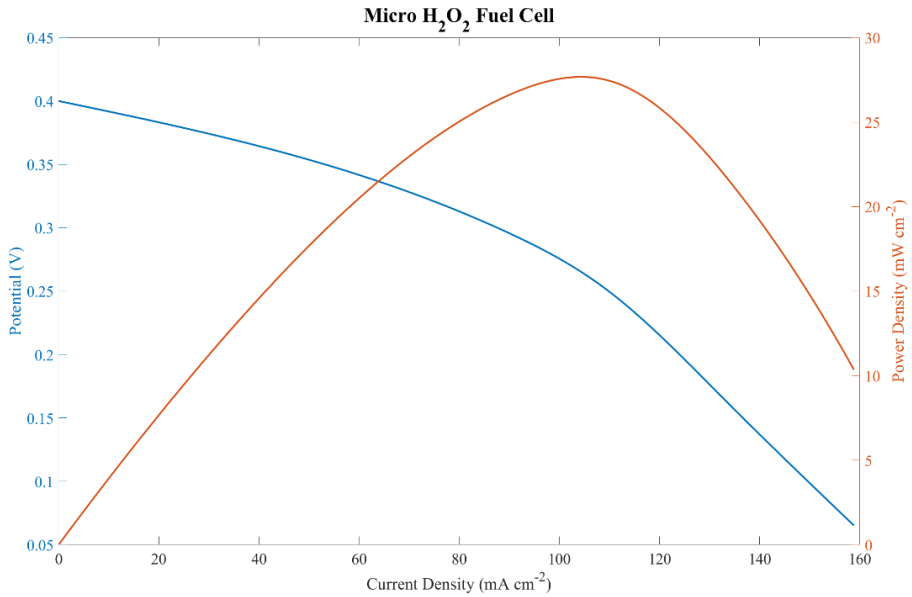

Figure 13: *Blue y-axis is polarization curve. Orange y-axis is power density curve. X-axis describes current density.*

5 Conclusion

In this project we were able to detail the process for creating a microfluidic fuel cell using two-photon lithography and electrodeposition. First, we studied and functionalized the writing parameters for two-photon lithography with the Nanoscribe on patterned metal surfaces—creating a regression response surface applicable to metal substrates. Second, we studied how to perform a quality electrodeposition of Nickel and WO_3 in micron-scale interstices of multiple levels in a 3D structure—discovering the main parameters that affect the deposition and determing a suitable variable space for these parameters. Lastly, we measured the performance of the H_2O_2 single compartment microfluidic fuel cell and were able to obtain power densities (mW cm^{-2}) that exceed literature values by a factor of two[9] and volumetric power densities (W cm^{-3}) comparable to solid oxide fuel cells[10].

6 Future Work

For the promising results we have now, we will continue to research in this path to finish more goals we haven't achieve due to time limit in this quarter. First, we will design more types of nanostructure with high surface area and enough gaps for Ni deposition to go deep into the bottom of the structure. We'll see how the increasing surface area and number of structure layers will help the cell performance. Second, we will improve Ni deposition process by trying different types of solution recipes, for example, using nickel acetate or nickle chloride instead or with nickel sulfate, changing reducing agent to sodium borohydride or sodium phosphite and control the amount of surfactant to limit generating scum layer. Current cycles and amount will also be adjusted to achieve more steady Ni deposition. Last but not least, we will improve WO_3 catalytic performance by adjusting the surface area in cathode or improve electrodeposition method to create more W metal in WO_3.

7 Acknowledgement

We cannot express enough thanks to all SNF community staffs for their financial and technical support and encouragement. Swaroop gave us a lot of good advice on using choosing equipment and training sections. Tony is an expert in electro chemistry and advised us on improving our Ni deposition. Also, thank to Usha, Lavendra, Graham, Cliff, Maurice who trained us on different equipment on time so that we are able to catch the deadline. Thanks to all the students who let us shadow, specially Pingyu who helped us a lot on Nanoscribe. Very special thanks to our PI Xiaolin Zheng for all the chemicals and Gamry 1010B Potentiostat for Ni deposition.

8 Budget

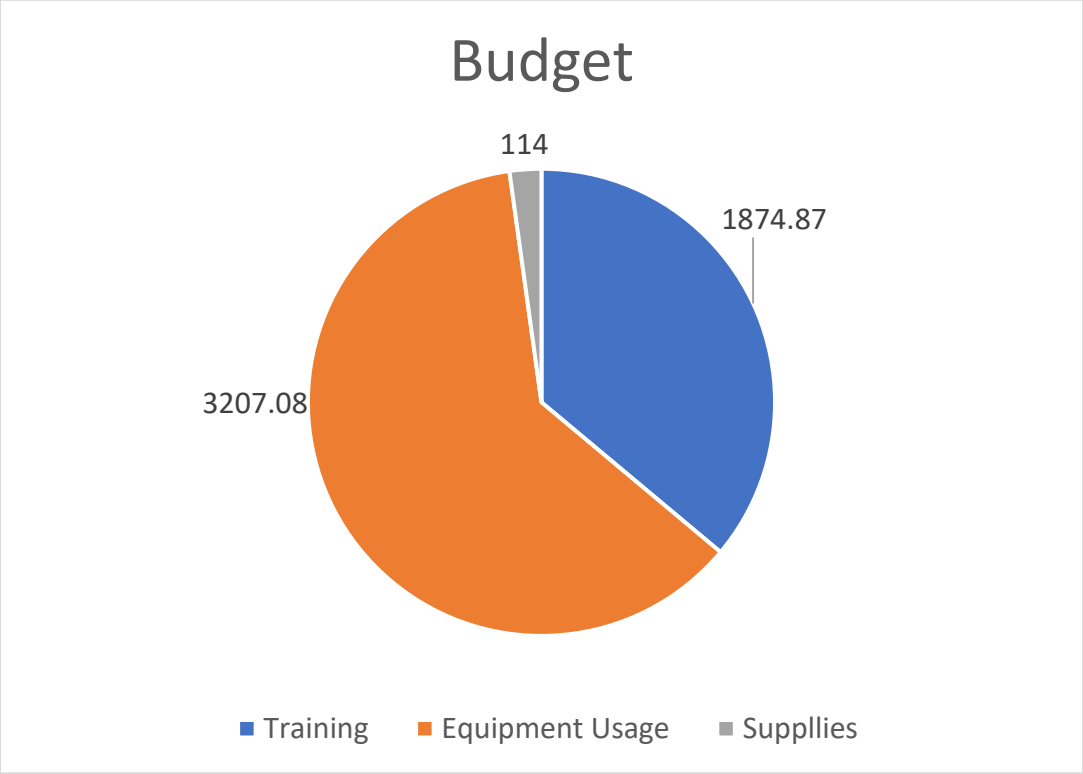

Total Cost: 5195.95

9 References

[1] Liang An, T. Z. (2014). The dual role of hydrogen peroxide in fuel cells. *Engineering Sciences*, 55-64.
[2] McDonnell-Worth, C. J. (2018). Progress Towards Direct Hydrogen Peroxide Fuel Cells (DHPFCs) as an Energy Storage Concept. *Australian Journal of Chemistry*, 781-788.
[3] J. D Plummer and P.B. Griffin, "Silicon and Compound Semiconductor Fabrication Technologies", *Stanford University*, Not Published .
[4] V. Harinarayana, Y. Shin (2021). Two-photon lithography for three-dimensional fabrication in micro/nanoscale regime: A comprehensive review. *Optics & Laser Technology*, 142
[5] Nanoscribe GmbH (2015).Nanoscribe Photonic Professional (GT) User Manual.
[6] Nickel Institute (2014). Nickel Plating Handbook.
[7] G. Hong, A. Holmes, M. Heaton (2003). SU-8 Resist Plasma Etching And Its Optimization. *Imperial College, London, Uk*
[8] M. Arslan, Y. First, S. Tokgoz, A. Peksoz (2021). Fast Electrochromic Response And High Coloration Efficiency Of Al-Doped WO_3 Thin Films For Smart Window Applications. *Ceramics International*, 32570-32578
[9] S. Wang, D. Ye, Z. Liu, X. Zhu, R. Chen, Q. Liao, Y. Yang, H. Liu (2022). A Flexible On-Fiber H2O2 Microfluidic Fuel Cell With High Power Density. *International Journal of Hydrogen Energy*, 4793-4803
[10] H. Sui and H. Ren, "A Miniaturized Planar Solid Oxide Fuel Cell Based on Stainless Steel Microfluidic Channels,"*2022 IEEE 35th International Conference on Micro Electro Mechanical Systems Conference (MEMS)*, 2022, pp. 632-635